Applied Catalysis B: Environmental 188 (2016) 48–55

Contents lists available at ScienceDirect

Applied Catalysis B: Environmental

journal homepage: www.elsevier.com/locate/apcatb

Visible-light photocatalytic oxidation of CO over plasmonic Au/TiO_2: Unusual features of oxygen plasma activation

Xiao-Qing Deng[a,b], Bin Zhu[a,b], Xiao-Song Li[a,b], Jing-Lin Liu[a,b], Xiaobing Zhu[a,b,*], Ai-Min Zhu[a,b,*]

[a] Laboratory of Plasma Physical Chemistry, Dalian University of Technology, Dalian 116024, China
[b] Center for Hydrogen Energy and Liquid Fuels, Dalian University of Technology, Dalian 116024, China

ARTICLE INFO

Article history:
Received 28 September 2015
Received in revised form 19 January 2016
Accepted 24 January 2016
Available online 28 January 2016

Keywords:
Au/TiO_2 photocatalyst
Visible light
Plasma activation
LSPR
CO oxidation

ABSTRACT

To seek an efficient activation of plasmonic Au/TiO_2 photocatalysts, atmospheric-pressure cold plasmas of oxygen (OP) and argon (ArP) were employed to activate the Au/TiO_2 coating samples on glass substrate and compared with the conventionally calcination. The activated samples were evaluated in a continuous-flow photocatalytic oxidation (PCO) reactor under visible light ($\lambda > 420$ nm) for CO removal from synthetic air and characterized by transmission electron microscopy (TEM), X-ray photoelectron spectroscopy (XPS), UV–vis spectroscopy, CO chemisorption and electron paramagnetic resonance (EPR). Although Au nanoparticles (NPs) of the three activation samples averaged at around 4 nm by TEM, the OP and ArP samples exhibited the highest and lowest PCO activity, respectively. An unusual feature of oxygen plasma activation is high content of surface oxygen, which favors superoxide (O_2^-) formation by accepting hot electron generated from absorption of visible light through local surface plasmon resonance (LSPR) of Au NPs. The OP sample has the lowest metallic Au content but its cationic Au can be rapidly reduced to form numerous low-coordinated metallic Au around the interface between Au NPs and TiO_2 support in the induction period, which is another unusual feature of oxygen plasma activation.

1. Introduction

Photocatalysis has become a very promising technology for environmental and energy applications in recent decades, due to its environment friendly, energy saving and high efficiency [1]. TiO_2 as the most common photocatalysts, however, has a large band gap energy (3.2 eV for anatase and 3.0 eV for rutile), which limits its application in the visible region accounted for approximately 45% of terrestrial sunlight. To solve the problem, Au/TiO_2 as a visible-light photocatalyst has attracted much attention, because it has strong visible-light absorption via local surface plasmon resonance (LSPR) of Au nanoparticles (NPs). The visible-light activity of plasmonic Au/TiO_2 photocatalysts can be rationalized by the hot-electron transfer mechanism [2–7], which hot electrons are generated by absorption of visible light on Au NPs through LSPR effect and transfer to the conduction band of TiO_2.

For preparation of a highly active Au/TiO_2 catalyst or photocatalyst, deposition-precipitation and impregnation are the common methods, where the as-prepared state presents mainly Au^{3+} species [8] and should be activated to reduce Au^{3+} species. Generally, air calcination is employed to activate Au/TiO_2 for CO oxidation. However, there exists an attendant risk of Au NPs sintering for calcination because the melting temperature of Au NPs with a diameter of 2 nm is approximately as low as 600 K [9]. To avoid the sintering risk during Au/TiO_2 activation, cold plasma is very likely to be an alternative technique for Au/TiO_2 activation. In cold plasma, it is frequently preferable to energize free electrons and the energized electrons collide with atoms/molecules to make them excitation and ionization while keeping the gas cold. In our previous work, atmospheric-pressure cold plasma (abbreviated as "plasma" below) has been successfully applied in in-situ regeneration [10,11] and activation [12] of Au/TiO_2 for conventionally catalytic oxidation of CO. However, to our knowledge, Au/TiO_2 activated by plasma for photocatalytic application has not yet been reported. In this work, oxygen and argon plasmas were employed to activate Au/TiO_2 photocatalysts for CO removal from air under visible-light irradiation and compared with the conventionally calcination. Thereby, unusual features of oxygen

* Corresponding authors at: Laboratory of Plasma Physical Chemistry, Dalian University of Technology, Dalian, 116024, China.
E-mail addresses: xzhu@dlut.edu.cn (X. Zhu), amzhu@dlut.edu.cn, amzhu2009@gmail.com (A.-M. Zhu).

http://dx.doi.org/10.1016/j.apcatb.2016.01.055
0926-3373/

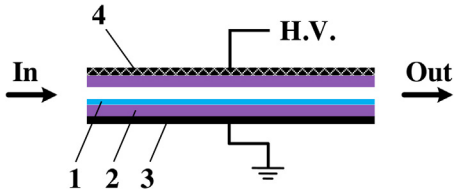

Fig. 1. Schematic diagram of plasma activation for Au/TiO_2 coating. 1-Au/TiO_2 coating on glass substrate, 2-quartz sheet, 3-aluminum foil, 4-stainless steel mesh.

plasma activation for plasmonic Au/TiO_2 photocatalysts were reported.

2. Experimental

2.1. Preparation and activation of Au/TiO_2 photocatalysts

Au/TiO_2 photocatalysts were prepared by a modified impregnation method [11,13]. The TiO_2 support (P25, Degussa) of 1.0 g was impregnated with a 2.2 mL aqueous solution of $HAuCl_4$ (2.43×10^{-2} mol/L). It was aged at room temperature for 12 h and washed twice with an aqueous ammonia solution (pH 8) and subsequently washed twice with deionized water. After washing, the filtered cake was dried at 80 °C for 8 h to obtain the as-prepared powder of Au/TiO_2. The actual Au content in the as-prepared powder was about 0.90 wt.%, determined by inductively coupled plasma-atomic emission spectroscopy (ICP-AES, Optima 2000DV, USA).

The as-prepared powder of 40 mg was added into 2 mL deionized water, and sonicated for 15 min. The slurry was coated by dip-coating method on a glass substrate of 75 mm (L) × 25 mm (W) × 1 mm (T). The substrate with the coating was dried at 80 °C for 1 h to obtain the as-prepared coating sample (no activation, designated as NA). The weight of the NA sample equals 35 ± 2 mg, which was obtained by subtracting the substrate weight from the total weight. Then, the NA samples were activated by O_2 plasma, Ar plasma and air calcination (held at 200 °C for 2 h, heating rate of 5 °C/min from room temperature) and marked as the OP, ArP and C200 samples, respectively. As expected, the scanning electron microscopy (SEM) images of the OP, ArP and C200 samples show that the Au/TiO_2 coatings appear to be almost evenly distributed onto the substrate besides small amount of agglomeration (Fig. S1 of the supporting information).

The plasma was generated by dielectric barrier discharge (DBD) with planar electrode configuration and two quartz sheets (1-mm thickness) as dielectric barrier at atmospheric pressure, as shown in Fig. 1. A stainless steel mesh of 75 mm (L) × 25 mm (W) covered the upper quartz sheet and was used as the high-voltage electrode; an aluminum foil of 75 mm (L) × 25 mm (W) was stuck to the lower quartz sheet and used as the ground electrode. The gap between the two quartz sheets is 2 mm. The plasma activation was under the conditions of 5 W input power, 1.8 kHz AC high-voltage frequency, 30 min discharge time and 100 mL/min gas flow rate of O_2 or Ar.

2.2. Photocatalytic testing

The schematic diagram of the experimental setup for photocatalytic oxidation (PCO) of CO was shown in Fig. 2. A testing coating sample was placed into a continuous-flow PCO reactor reported previously [14], with a quartz window (25 mm × 75 mm) to allow visible-light irradiation. A 300 W xenon lamp with a 420 nm cut-off filter was used as visible-light source, whose emission spectra was recorded by a monochromator (SR-750-B1, Andor, UK) and shown in the Inset of Fig. 2. It was confirmed that the irradiation did be visible light with wavelength longer than 420 nm. The light intensity onto the coating sample was 478 mW/cm^2, measured by a PM100USB optical power and energy meter with S302C thermal power sensor (Thorlabs, USA). The PCO reactor was cooled by water to keep the temperature of the coating sample at 13–14 °C measured by a thermocouple below it. The synthetic air (80% N_2 + 20% O_2) containing ~1000 ppm CO with a total flow rate of 250 mL/min was used as the reactant gas. CO and CO_2 concentrations were analyzed by a CO_x analyzer (S710, Sick/Maihak, Germany). The PCO experiments were conducted according to the following sequence. First, the Xe lamp was turned on and the O_2 gas at a flow rate of 250 mL/min as purging gas flowed into the PCO reactor till CO and CO_2 concentrations approached to baseline. Then, the reactant gas was switched into the reactor under the visible-light irradiation for starting PCO reaction. After the PCO reaction lasted for about 40 min, the Xe lamp was turned off to allow starting dark reaction.

CO conversion was defined as below:

$$\text{CO conversion}(\%) = \frac{C_{CO}^{in} - C_{CO}^{out}}{C_{CO}^{in}} \times 100\%$$

where C_{CO}^{in} and C_{CO}^{out} represent the concentrations of CO in inlet and outlet gases, respectively.

2.3. Catalyst characterization

The particle size of the OP, ArP and C200 samples after 30-min PCO were observed by transmission electron microscopy (TEM, Tecnai G220 S-Twin G220 S-Twin, FEI, USA) operating at 200 kV. The samples for TEM were prepared as follows: about 20 mg fine powders mixed with 5 mL ethanol to make a suspension for 15 min ultrasonic treatment; subsequently, five drops of the suspension were dripped on a copper grid with carbon polymer and dried at room temperature for measurement. The particle size distribution was calculated by counting more than 200 particles in different areas of the TEM images.

Surface chemical states of Au/TiO_2 catalysts were characterized by X-ray photoelectron spectroscopy (XPS, ESCALAB250 Thermo VG, USA.) using an Al Kα X-ray source (1486.6 eV) operated at 15 kV and 300 W. The samples were evacuated in the fore-chamber of the XPS spectrometer to 10^{-5} Pa and then transferred to the analytical chamber for analysis under 10^{-8} Pa. The binding energy was calibrated according to the XPS peak of carbon 1s at 284.6 eV.

UV–vis diffuse reflectance spectra (DRS) were conducted on the air-exposed Au/TiO_2 samples using lambda 750s spectrometer (Perkin-Elmer, USA) in the wavelength range of 200–800 nm. A background reference was taken using barium sulfate before the measurement.

The in-situ diffuse reflectance infrared Fourier transform (DRIFT) spectra of CO adsorption were recorded by an FT-IR spectrometer (Tensor 27, Bruker, Germany) with a MCT detector at a resolution of 4 cm^{-1} from 4000 to 1000 cm^{-1}. Prior to CO adsorption, the Au/TiO_2 samples placed in a DRIFT cell (equipped with CaF_2 windows) were pretreated with 100 mL/min He at 80 °C for 30 min and then cooled down to the room temperature. The background spectra were first collected at room temperature in He flowing (100 mL/min). Subsequently, CO adsorption was carried out by switching 1000 ppm CO/He (100 mL/min) into the DRIFT cell.

The amount of CO adsorbed on the surface of the Au/TiO_2 catalyst was measured at −106 °C in AutoChem II 2920 (Micromeritics, USA) automated system with CO pulse chemisorption method. Before chemisorption, the Au/TiO_2 samples were pretreated as follows: the sample (250 mg) was first treated in He flow (30 mL/min) at 80 °C for 30 min and then cooled down to the ambient temperature. To prevent the CO chemisorption on cation sites of TiO_2 support, hydration treatment were subsequently performed by

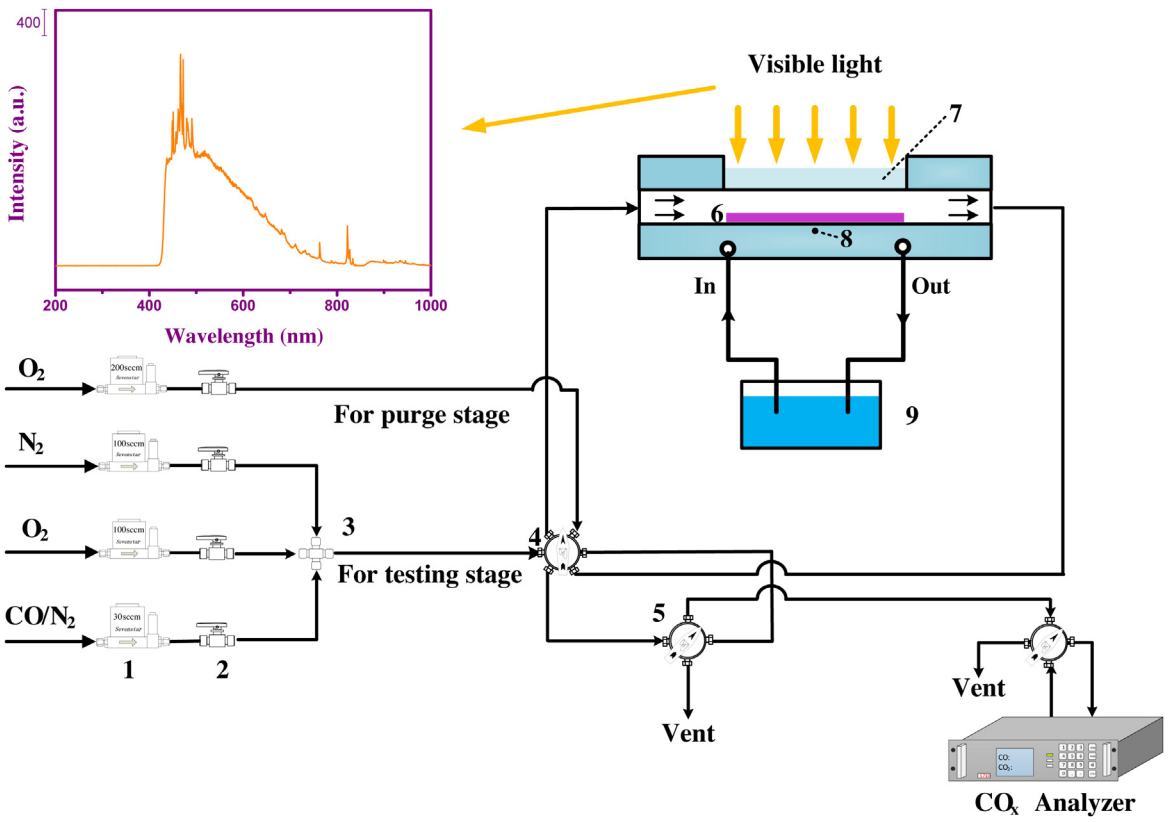

Fig. 2. Schematic diagram of the experimental setup of PCO. 1-Mass flow controller, 2-two-way valve, 3-union cross, 4-six-way valve, 5-four-way valve, 6-coating sample, 7-quartz window, 8-thermocouple, 9-cooling water bath. Inset: emission spectra of Xe lamp with a 420 nm cut-off filter.

pulsing He flow (10 mL/min) saturated with water over the samples at ambient temperature. After above pretreatment, the sample was cooled in He flow (30 mL/min) to −106 °C (attained by an ethanol-liquid nitrogen cryogenic mixture) for CO chemisorption. In CO chemisorption experiment, pulses of 2% CO/He (30 mL/min) were injected from a calibrated loop (50 μL) over the Au/TiO_2 samples, and the time interval between pulses was 7 min. CO chemisorption was assumed to be completed after three successive peaks showed the same peak area.

Electron paramagnetic resonance (EPR) measurements were carried out on a Bruker A200 spectrometer (Bruker A200, Bruker, USA) to test the reactive oxygen species produced by Au/TiO_2 samples. To prepare the samples for EPR, about 5 mg of Au/TiO_2 was first dispersed in 0.5 mL of methanol. Then, 18 μL of 5,5-dimethyl-1-pyrroline-N-oxide (DMPO, Sigma Chemical Co.) as the spin traps was added into this slurry. A suspension was finally obtained after homogenization of the slurry in an ultra-sound bath for 15 min. 0.1 mL of the suspension were injected into the quartz capillary by syringe for testing. To detect the response of reactive oxygen species generated from samples for the visible light irradiation, a 100 W mercury light lamp (λ > 420 nm) was applied during the testing process. The parameters of EPR measurement were set as below: center filed, 3320 G; sweep width, 160 G; microwave frequency, 9.32 GHz; power, 9.99 mW.

3. Results

3.1. Photocatalytic performance

To evaluate their visible-light PCO performance, the variations in CO conversion with time-on-stream (TOS) over the OP, ArP, C200 and NA samples of Au/TiO_2 with or without (dark) irradiation are illustrated in Fig. 3. It can be observed that the visible-light irradiation can significantly enhance the CO conversion for all the Au/TiO_2 samples due to the LSPR of Au NPs [12,15]. As shown in Fig. 3, the as-prepared sample (NA) only obtained ~30% CO conversion under visible-light irradiation and ~8% CO conversion in dark reaction. This means that, if without activation, the as-prepared sample would present a poor photocatalytic performance. Thus, the activated Au/TiO_2 samples were compared and discussed in the following sections. For Au/TiO_2 sample activated by calcination (C200), its CO conversion decreased rapidly from the maximum

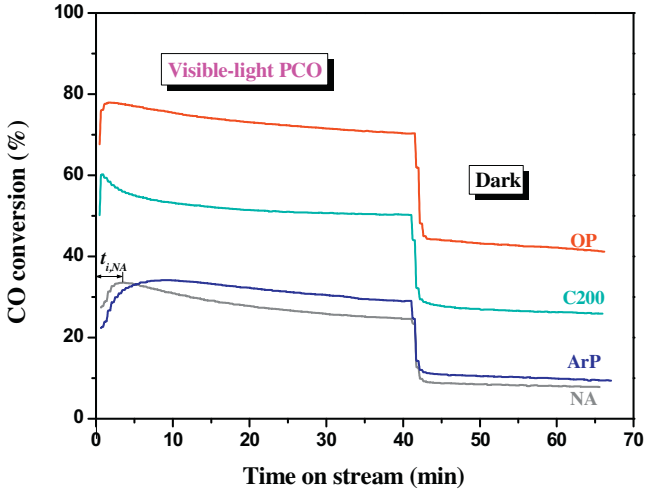

Fig. 3. Conversion of CO versus TOS over the OP, ArP, C200 and NA samples with or without visible-light irradiation. $t_{i,NA}$ represents the induction period of the NA. Reaction conditions: 1000 ppm CO in synthetic air, $\tau = 0.45$ s, $F = 250$ mL/min.

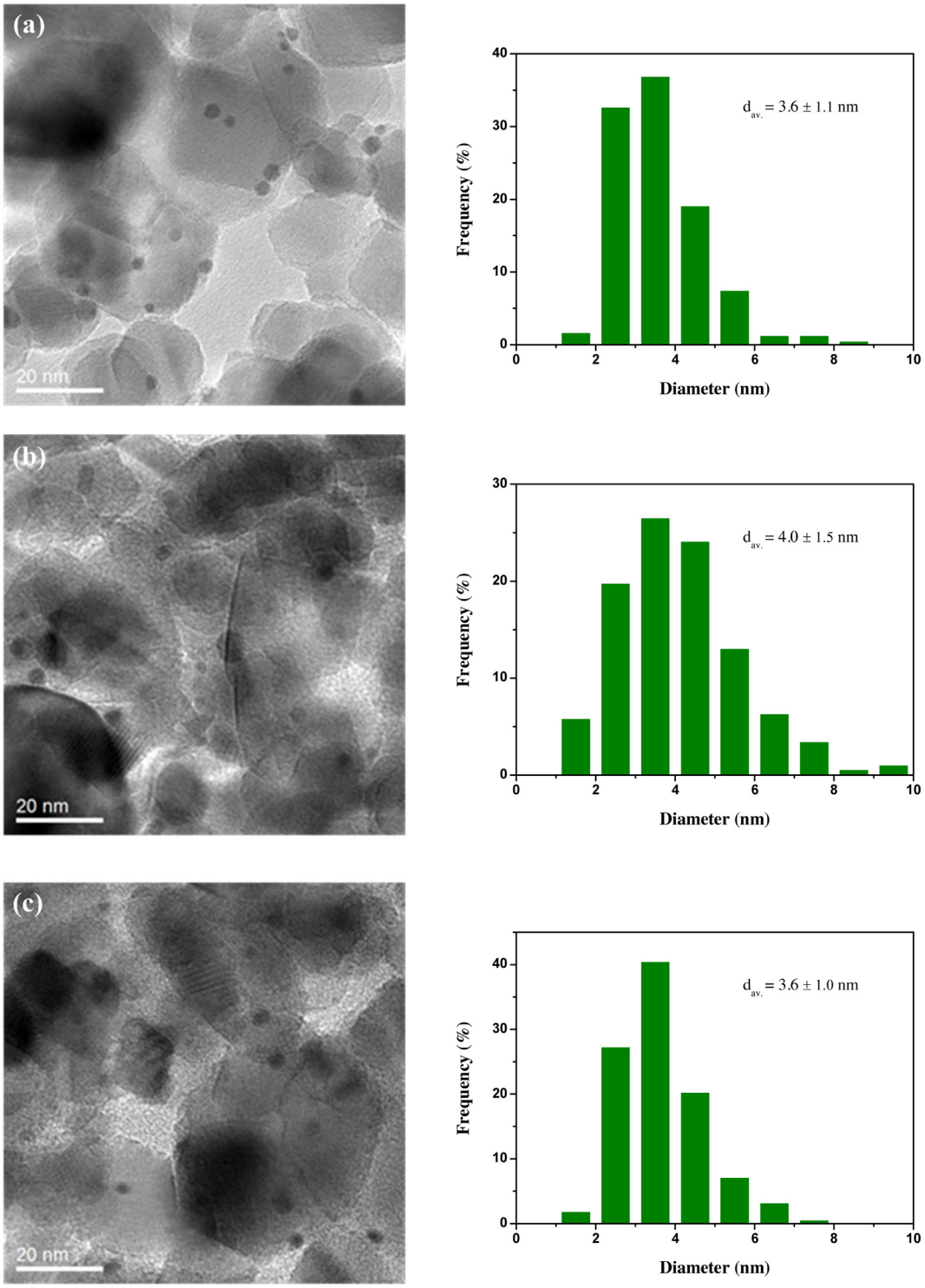

Fig. 4. TEM images and the associated particle size histograms of the (a) C200, (b) ArP and (c) OP samples.

(60%) in a few minutes and followed by a slight decrease (almost at 50%) in visible-light PCO reaction, whereas CO conversion was only 28% in dark reaction. Notably, the O_2 plasma activated sample (OP) exhibited the highest CO conversion among these samples. The CO conversion of the OP sample did not have the fast decline as shown in the C200 sample and decreased slowly from the maximum of 78% to 71% at TOS of 40 min under visible-light irradiation, which is much higher than that of the C200 sample. It is suggested that O_2 plasma is an effective activation approach for plasmonic Au/TiO_2 visible-light photocatalysts. Nevertheless, the Ar plasma activated sample (ArP) only showed a poor performance similar to the NA sample. This indicates that the effect of plasma activation on Au/TiO_2 photocatalyst strongly depends on the gas composition of plasma. It is worth noting that, for the Au/TiO_2 samples, there exists an induction period [16] and the induction period of the NA sample, $t_{i,NA}$, was indicated in Fig. 3 as an example. The OP and C200 samples showed a very shorter induction period than the ArP and NA samples. In this study, the induction period is likely attributed

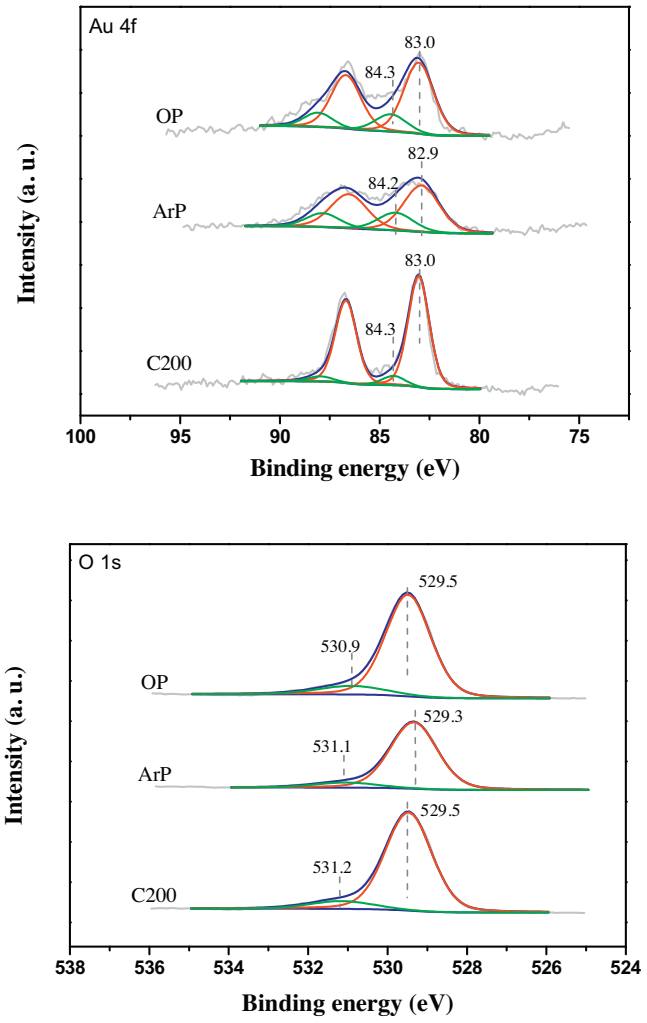

Fig. 5. XPS spectra of Au 4f and O 1s for the OP, ArP and C200 samples after PCO reaction.

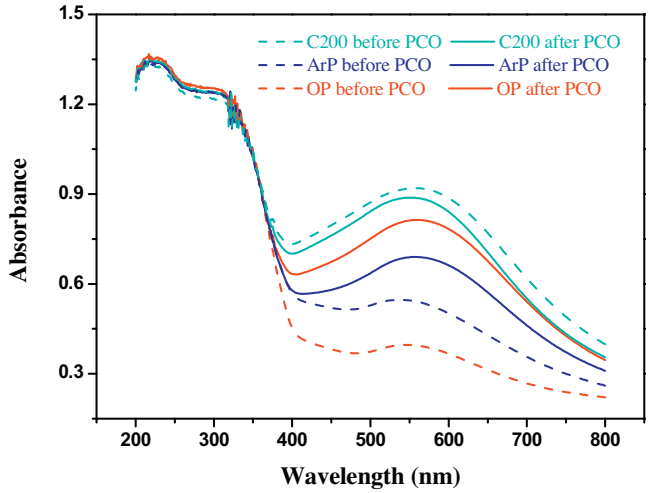

Fig. 6. UV–vis diffuse reflection spectra of the OP, ArP and C200 samples.

to the reduction of cationic Au during CO oxidation, which will be discussed in Section 4.

In order to understand the relationship between photocatalytic performance and physicochemical properties of the Au/TiO_2 samples, the particle size, chemical state, optical property and CO adsorption of the Au/TiO_2 samples were characterized by various techniques, including TEM, XPS, UV–vis DRS, in-situ DRIFT and low-temperature CO pulse chemisorption.

3.2. TEM observation

Since the size of the Au particle played an important role in determining their photocatalytic activity [17], the Au particle size of the activation samples after PCO reaction was measured, the typical TEM images and the size distribution of Au particles are presented in Fig. 4. It can be clearly seen that the Au particle size of all the samples showed no distinct difference and averaged at around 4 nm, indicating that the Au particle size of all the samples were in the optimal range below 5 nm for the highly active Au/TiO_2 visible-light photocatalyst [18,19].

3.3. Surface chemical state analysis

The high resolution XPS measurements for the activation samples before and after PCO reaction were performed to examine their surface chemical state. It should be noted here that we mainly focus on analyzing the chemical valence of Au species and the surface oxygen species because they are two crucial factors for determining the activity of plasmonic Au/TiO_2 photocatalyst [20]. The XPS spectra of Au 4f and O 1s are shown in Fig. 5, and the corresponding results for Au/TiO_2 samples before and after PCO were summarized in Table 1. After fitting analysis, as shown in Fig. 5, the XPS spectra of the Au 4f can be deconvoluted into Au^0 and Au^+ [12]. As shown in Table 1, the calcined Au/TiO_2 sample possesses a high metallic Au content of 91.7%, indicating almost complete reduction of the cationic Au under calcination. Meanwhile, there is a distinct change in the metallic Au contents of the OP and ArP samples before and after PCO reaction. The metallic Au contents of the ArP and OP samples were 68.0% and 57.6% before PCO, respectively, suggesting that the only a portion of cationic Au were reduced to metallic Au during plasma activation. Moreover, owing to its oxidative atmosphere, the OP sample shows a lower metallic Au content than that of the ArP sample before PCO reaction. However, after PCO, the metallic Au content of the ArP and OP samples increased to 72.8% and 79.8%, respectively, indicating the occurrence of cationic Au reduction in the induction period. In order to evaluate the dispersion of Au for the Au/TiO_2 photocatalysts, Au/Ti ratios obtained from XPS data were also listed in Table 1. It can be seen that there was no remarkable difference among the samples, which may be attributed to the low Au loading of Au/TiO_2 in this work.

In the case of O 1s spectra (Fig. 5), the peaks at ~529.3 eV [21] and ~531.0 eV [22,23] were assigned to the lattice oxygen $[O]_l$ and surface oxygen $[O]_s$, respectively. Furthermore, the surface oxygen species of the fresh samples (before PCO) are located on both Au NPs and TiO_2 support. The surface oxygen species on Au NPs are rapidly consumed by CO during the induction period, which leads to the decrease in the surface oxygen content of the used samples (after PCO) in comparison with the fresh samples (Table 1). However, the surface oxygen on TiO_2 can remain at a relatively stable content due to its cycle of formation and consumption during the PCO reaction. The distribution of the oxygen species for all the samples (as shown in Table 1) also shows that the O_2 plasma activated sample presents much higher $[O]_s$ content than the ArP and C200 samples, especially before PCO reaction. Meanwhile, the ArP and C200 samples possess a similar surface oxygen content before and after PCO reaction. Indeed, it has been reported that O_2 plasma treatment favors formation of surface oxygen species on catalysts, and the generated surface oxygen plays an important role in oxidation reaction [24–26]. The large amount of surface oxygen for the OP sample is a plausible explanation for its high photocatalytic

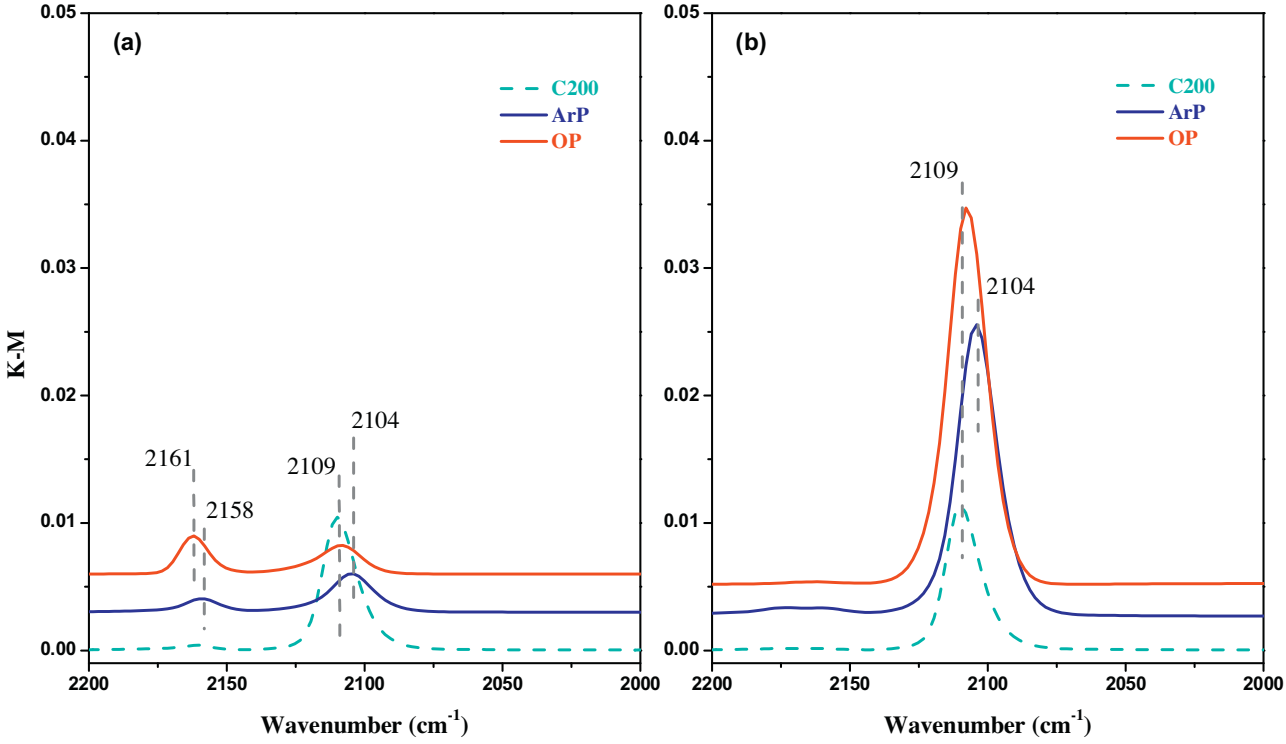

Fig. 7. In-situ DRIFT spectra of CO adsorption at exposure time of (a) 2 min and (b) 7 min. Adsorption conditions: 1000 ppm CO/He, 100 mL/min, 20 °C.

Table 1
XPS analysis of the Au/TiO_2 samples Proportion (at.%).

Samples	Peak position of Au (eV)		Proportion (at.%)		
	Au^0 $4f_{7/2}$	Au^+ $4f_{7/2}$	$[O]_s/([O]_s+[O]_l)$	$Au^0/(Au^0+Au^+)$	Au/Ti
C200 before PCO	83.0	84.3	17.7	91.7	0.021
C200 after PCO	83.0	84.3	9.7	92.5	0.020
ArP before PCO	82.9	84.2	14.4	68.0	0.023
ArP after PCO	82.9	84.2	9.3	72.8	0.020
OP before PCO	83.0	84.3	23.1	57.6	0.022
OP after PCO	83.0	84.3	11.2	79.8	0.020

activity, as the sufficient surface oxygen not only can directly provide active oxygen species for CO oxidation but also favors the LSPR by accepting hot electron transferred from photoactivated Au particles [2], and the corresponding mechanism will be discussed in Section 4.

3.4. Optical property

Since the promotion of visible-light on CO oxidation reaction arises from a resonant oscillation of free electrons coupled by visible-light, i.e. LSPR, it is essential to investigate the photo-responsive behaviors of the Au/TiO_2 samples. Fig. 6 shows the UV–vis diffuse reflectance spectra of the C200, ArP and OP samples. Obviously, the typical LSPR absorption band of metallic Au NPs centered at ca. 560 nm can be observed for all samples [27,28]. The C200 sample shows a strong plasmon band of metallic Au particle before and after PCO reaction due to its high content of metallic Au. For plasma activated Au/TiO_2 samples, their metallic gold plasmon band were dramatically enhanced after PCO reaction because of the reduction of cationic Au during PCO reaction. Before PCO, the OP sample shows a weaker absorption band at ca. 560 nm compared with the ArP sample, which results from its relatively lower content of metallic Au. However, after PCO reaction, the LSPR absorption band of the OP sample became more intensive than that of the ArP sample, which means that the cationic Au in the O_2 plasma activated sample might be much easier to be reduced during the induction period. The above UV–vis results are in a good agreement with the XPS results.

3.5. CO chemisorption

The chemisorption behavior of CO reactant on the Au/TiO_2 samples were investigated. Fig. 7 shows the evolution of DRIFT spectra of CO adsorbed on the OP, ArP and C200 samples at room temperature (~20 °C). As shown in Fig. 7a, at a short exposure time (2 min), the C200 sample only shows the band at 2109 cm^{-1} due to the linearly adsorbed CO on Au^0 [29–32]. For the plasma activated samples, apart from the band of CO adsorbed on Au^0 (2100–2110 cm^{-1}), there appeared a new weak band at around 2160 cm^{-1}, which can be assigned to the CO adsorbed on Au^+ [33–35]. The peak of CO adsorbed on Au^+ of the OP was stronger than that of the ArP, inferring that Au^+ content of the OP was higher than that of the ArP, which was consistent with the results of XPS and UV–vis spectra. However, after a long exposure time (7 min, Fig. 7b), the band of CO adsorbed on Au^+ rapidly disappeared along with the significant intensification of the band of CO adsorbed on Au^0, indicating that the cationic gold in the plasma activated samples were fast reduced to metallic Au by CO. In addition, the bands of CO adsorbed on Au^0

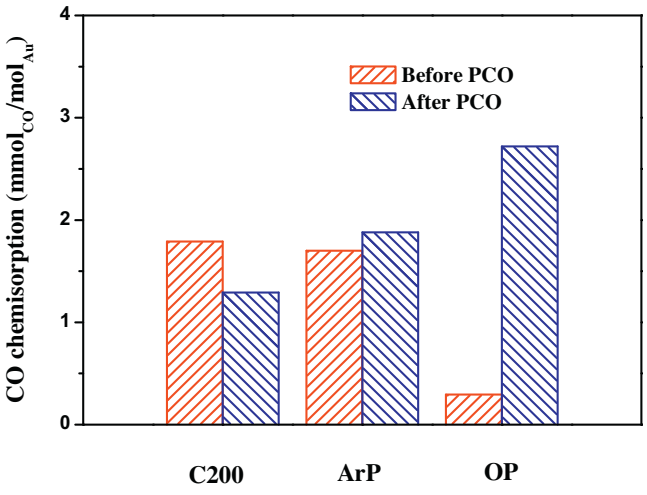

Fig. 8. Quantitative CO chemisorption at −106 °C.

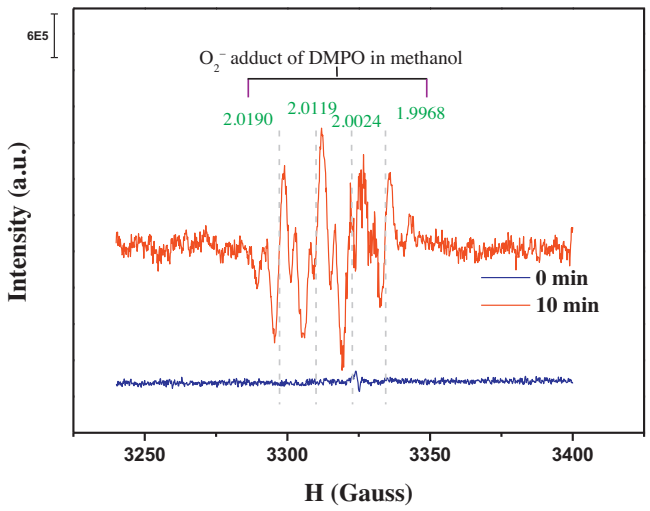

Fig. 9. EPR spectra of superoxide radical species trapped by DMPO on the OP sample in the methanol under visible-light irradiation.

for the plasma activated samples are much more intensive than that of the C200 sample, inferring their more adsorption sites towards CO than the C200. Interestingly, distinct from those of the OP and C200 samples, the bands of the ArP shifted to lower frequency due to CO adsorbed on its electron-rich metallic gold sites [36,37]. It can be reasonably inferred that, for the ArP sample, CO adsorption sites on Au NPs are far from the interface between Au NPs and TiO_2 support due to its plasma activation in an inert environment. By contrast, the OP and C200 samples provide electron-deficient metallic gold sites for CO adsorption, which are near to the interface between Au NPs and TiO_2 support. This is probably caused by the action of surface oxygen on TiO_2 support around the perimeter Au NPs in their activation of an oxidative environment.

The capability of CO chemisorption on these samples was determined by using the low-temperature CO pulse chemisorption technique [38,39] and shown in Fig. 8. The results presented in Fig. 8 clearly indicate there existed a distinct CO chemisorption capacity between the conventional calcined and O_2 plasma activated samples. Owing to its low metallic Au content, the OP sample before PCO reaction showed much lower CO uptakes (0.3 $mmol_{CO}/mol_{Au}$) than the C200 (1.8 $mmol_{CO}/mol_{Au}$), which is consistent with its much weaker intensity of band at 2109 cm^{-1} shown in Fig. 7a. However, after cationic Au reduction in PCO reaction, the plasma activated samples possess much higher CO uptake than that of the C200, especially the O_2 plasma activated sample reaches 2.7 $mmol_{CO}/mol_{Au}$. Although the plasma activated samples show a lower content of metallic Au after PCO reaction, they exhibit higher CO chemisorption capacity than the C200. This can be explained that their larger amount of low-coordinated Au species favors CO adsorption [34,40], which would play a crucial role in enhancing photocatalytic activity of the OP sample. Here, the large amount of low-coordination sites for the OP sample may be ascribed to its very small Au clusters or even isolated Au atoms originated from O_2 plasma activation. Nevertheless, due to the very small particle size of these Au clusters, they were not detected by the TEM in this study.

4. Discussion

Au/TiO_2 has been extensively studied as a plasmonic visible-light photocatalyst for a variety of oxidation reaction [41,42]. Generally, the performance of Au/TiO_2 photocatalyst critically depends on Au NPs and surface oxygen. The Au NPs supported on TiO_2 not only are directly related to the LSPR effect but also determine the catalytic activity of the Au/TiO_2 as the active sites in oxidation reaction [43,44]. On the other hand, the surface oxygen can be reduced into surperoxide (O_2^-) by hot electron in TiO_2 conduction band transferred from the photoexcited Au^0 to participate in the oxidation reaction [19,45,46]. It is prevalently accepted that the CO oxidation over Au/TiO_2 at low temperature follows a Langmuir-Hinshelwood mechanism [47,48]. That is, the CO adsorbed on Au NPs, while molecular oxygen adsorbed on oxygen vacancies (most probably on the interface between Au NPs and TiO_2) for forming superoxide (O_2^-) to react with the adsorbed CO. Apparently, large amount of adsorbed CO (especially on the sites of Au^0 near to the interface) and surface oxygen favor achievement of high activity. In addition, the active sites for CO oxidation were mainly related to the metallic Au rather than the Au cations [8,49–52]. Therefore, the induction period for the ArP and OP (as shown in Fig. 3) during CO oxidation reflects the reduction of cationic Au (as evidenced by XPS, UV–vis and DRIFT results) in plasma activated samples. It is worth noting that cationic Au reduction and the decrease of surface oxygen for the plasma activated samples should occur during the induction period.

The electron in metallic Au can be effectively excited by visible light due to its strong LSPR (Fig. 6) and thus separated from metallic Au (R1). Although some separated electron would recombine with the photoinduced Au^+ (R2), however, owing to their much higher energy level than that of TiO_2 conduction band, large amount of photoexcited hot electrons would overcome schottky barrier between the metallic Au and TiO_2 and transfer into TiO_2 conduction band. The electron in the conduction band can readily reduce the surface oxygen adjacent the metallic Au (most probably around the interface) to form superoxides (O_2^-) (R3) and then react on the interface with the spillover CO from Au (R4). Apparently, the LSPR of Au/TiO_2 under visible light irradiation can significantly enhance the activation of surface oxygen by forming large amount of O_2^- for CO oxidation on the interface, which can be evidenced by EPR analysis of the OP sample (Fig. 9) where the typical superoxide radical species trapped by DMPO on the OP sample in the methanol can be observed [53]. In addition, it is worth noting that the hot electrons might further react with superoxide to produce the more active O^- species due to the relatively high density of O_2^- on the interface under visible-light irradiation (R5) [54,55]. This favors higher rate of CO conversion (R6) [56].

$$Au^0 + h\upsilon \rightarrow Au^+ + e \quad (R1)$$

$$Au^+ + e \rightarrow Au^0 + h\upsilon \quad (R2)$$

$$O_2 + e \rightarrow O_2^- \quad (R3)$$

$$2CO + O_2^- \rightarrow 2CO_2 + e \quad (R4)$$

$$O_2^- + e \rightarrow 2O^- \quad (R5)$$

$$CO + O^- \rightarrow CO_2 + e \quad (R6)$$

In this study, the XPS and CO chemisorption results illustrate that the ArP after PCO reaction possesses the similar surface oxygen content but higher CO uptakes in comparison with the C200, however, it shows much lower activity than that of the C200 (Fig. 3). The poor PCO performance of the ArP is likely caused by its relatively low content of Au sites near to the interface. Although the OP after PCO reaction presents a lower content of metallic Au than the C200 (as illustrated by XPS and UV–vis results), it exhibits the highest activity among the three activated samples (Fig. 3). Based on the above mechanism, the highest photocatalytic activity of the OP sample for CO oxidation should be attributed to its highest content of surface oxygen (as evidenced by the XPS results) and largest amount of low-coordinated Au species near to the interface.

In short, we have demonstrated here that the O_2 plasma activation can dramatically enhance the visible-light PCO activity of Au/TiO_2 for CO oxidation. By comparing with the calcination and Ar plasma activated samples, it is believed that this remarkable improvement of O_2 plasma activation is mainly attributed to large amount of surface oxygen and low-coordinated Au species for CO adsorption around the interface between Au NPs and TiO_2 support, which would also play a very important role in other visible-light PCO reaction. This study thus provides a highly effective approach in activating the plasmonic visible-light photocatalysts.

5. Conclusions

Atmospheric-pressure cold plasmas of oxygen and argon were applied to activate plasmonic Au/TiO_2 photocatalysts and compared with the conventionally calcination at 200 °C. Among the three activation samples, the OP and ArP samples exhibited the highest and lowest visible-light PCO activity, respectively. TEM observation revealed that Au NPs of the three activation samples averaged at around 4 nm. According to XPS analysis, the OP sample has the highest content of surface oxygen and it readily forms superoxide (O_2^-) in PCO, which was evidenced by EPR measurement. XPS also revealed the OP sample has the lowest content of metallic Au but its cationic Au can be rapidly reduced in the induction period, which coincides with the characterizations of UV–vis spectra and CO chemisorption. The CO chemisorption capacity of the activated samples after PCO reaction is in the following sequence: OP > ArP > C200.

Acknowledgment

This work is supported by National Natural Science Foundation of China (11475041, U1201231).

Appendix A. Supplementary data

Supplementary data associated with this article can be found, in the online version, at http://dx.doi.org/10.1016/j.apcatb.2016.01.055.

References

[1] K. Nakata, A. Fujishima, J. Photochem. Photobiol. C: Photochem. Rev. 13 (2012) 169–189.
[2] Y. Tian, T. Tatsuma, Chem. Commun. (2004) 1810–1811.
[3] Y. Tian, T. Tatsuma, J. Am. Chem. Soc. 127 (2005) 7632–7637.
[4] A. Tanaka, S. Sakaguchi, K. Hashimoto, H. Kominami, ACS Catal. 3 (2013) 79–85.
[5] C. Gomes Silva, R. Juárez, T. Marino, R. Molinari, H. Garcíía, J. Am. Chem. Soc. 133 (2010) 595–602.
[6] K. Yang, J.-F. Liu, R.-R. Si, X. Chen, W.-X. Dai, X.-Z. Fu, J. Catal. 317 (2014) 229–239.
[7] J.-W. Tang, ChemSusChem 3 (2010) 800–801.
[8] J.H. Yang, J.D. Henao, M.C. Raphulu, Y.-M. Wang, T. Caputo, A.J. Groszek, M.C. Kung, M.S. Scurrell, J.T. Miller, H.H. Kung, J. Phys. Chem. B 109 (2005) 10319–10326.
[9] P. Buffat, J.-P. Borel, Phys. Rev. A 13 (1976) 2287–2298.
[10] H.-Y. Fan, C. Shi, X.-S. Li, S. Zhang, J.-L. Liu, A.-M. Zhu, Appl. Catal. B: Environ. 119–120 (2012) 49–55.
[11] B. Zhu, X.-S. Li, J.-L. Liu, J.-B. Liu, X. Zhu, A.-M. Zhu, Appl. Catal. B: Environ. 179 (2015) 69–77.
[12] S. Zhang, X.-S. Li, B. Zhu, J.-L. Liu, X. Zhu, A.-M. Zhu, B.W.L. Jang, Catal. Today 256 (2015) 142–147.
[13] L. Delannoy, N.E. Hassan, A. Musi, N.N. Le To, J.-M. Krafft, C. Louis, J. Phys. Chem. B 110 (2006) 22471–22478.
[14] X. Zhu, D.-L. Chang, X.-S. Li, Z.-G. Sun, X.-Q. Deng, A.-M. Zhu, Chem. Eng. J. 279 (2015) 897–903.
[15] J.-F. Liu, R.-R. Si, H.-R. Zheng, Q. Geng, W.-X. Dai, X. Chen, X.-Z. Fu, Catal. Commun. 26 (2012) 136–139.
[16] S. Zhang, X.-S. Li, B.-B. Chen, X.-B. Zhu, C. Shi, A.-M. Zhu, ACS Catal. 4 (2014) 3481–3489.
[17] T. Akita, P. Lu, S. Ichikawa, K. Tanaka, M. Haruta, Surf. Interface Anal. 31 (2001) 73–78.
[18] Y.-M. Wu, H.-B. Liu, J.-L. Zhang, F. Chen, J. Phys. Chem. C 113 (2009) 14689–14695.
[19] D. Tsukamoto, Y. Shiraishi, Y. Sugano, S. Ichikawa, S. Tanaka, T. Hirai, J. Amer. Chem. Soc. 134 (2012) 6309–6315.
[20] M.P. Casaletto, A. Longo, A. Martorana, A. Prestianni, A.M. Venezia, Surf. Interface Anal. 38 (2006) 215–218.
[21] W.E. Slink, P.B. DeGroot, J. Catal. 68 (1981) 423–432.
[22] M. Shirkhanzadeh, J. Mater. Sci. Mater. Med. 6 (1995) 206–210.
[23] J. Biener, E. Farfan-Arribas, M.M. Biener, C.M. Friend, R.J. Madix, J. Chem. Phys. 123 (2005) 094705.
[24] Y. Teramoto, H.-H. Kim, A. Ogata, N. Negishi, Catal. Lett. 143 (2013) 1374–1378.
[25] O. Guaitella, C. Lazzaroni, D. Marinov, A. Rousseau, Appl. Phys. Lett. 97 (2010) 011502.
[26] U. Roland, F. Holzer, F.-D. Kopinke, Catal. Today 73 (2002) 315–323.
[27] R. Zanella, S. Giorgio, C.-H. Shin, C.R. Henry, C. Louis, J. Catal. 222 (2004) 357–367.
[28] C.J. Orendorff, T.K. Sau, C.J. Murphy, Small 2 (2006) 636–639.
[29] M.A. Bollinger, M.A. Vannice, Appl. Catal. B: Environ. 8 (1996) 417–443.
[30] J.C. Fierro-Gonzalez, B.C. Gates, Catal. Today 122 (2007) 201–210.
[31] M.-J. Li, Z.-L. Wu, Z. Ma, V. Schwartz, D.R. Mullins, S. Dai, S.H. Overbury, J. Catal. 266 (2009) 98–105.
[32] L. Li, A.-Q. Wang, B.-T. Qiao, J. Lin, Y.-Q. Huang, X.-D. Wang, T. Zhang, J. Catal. 299 (2013) 90–100.
[33] F. Boccuzzi, A. Chiorino, S. Tsubota, M. Haruta, J. Phys. Chem. 100 (1996) 3625–3631.
[34] F. Boccuzzi, A. Chiorino, J. Phys. Chem. B 104 (2000) 5414–5416.
[35] M.M. Schubert, A. Venugopal, M.J. Kahlich, V. Plzak, R.J. Behm, J. Catal. 222 (2004) 32–40.
[36] X.-Y. Liu, C.-Y. Mou, S. Lee, Y.-N. Li, J. Secrest, B.W.-L. Jang, J. Catal. 285 (2012) 152–159.
[37] M. Boronat, P. Concepción, A. Corma, J. Phys. Chem. C 113 (2009) 16772–16784.
[38] F. Menegazzo, M. Manzoli, A. Chiorino, F. Boccuzzi, T. Tabakova, M. Signoretto, F. Pinna, N. Pernicone, J. Catal. 237 (2006) 431–434.
[39] A. Chiorino, M. Manzoli, F. Menegazzo, M. Signoretto, F. Vindigni, F. Pinna, F. Boccuzzi, J. Catal. 262 (2009) 169–176.
[40] W.-L. Yim, T. Nowitzki, M. Necke, H. Schnars, P. Nickut, J. Biener, M.M. Biener, V. Zielasek, K. Al-Shamery, T. Klüner, M. Bäumer, J. Phys. Chem. C 111 (2007) 445–451.
[41] C.-L. Wang, D. Astruc, Chem. Soc. Rev. 43 (2014) 7188–7216.
[42] S. Linic, P. Christopher, D.B. Ingram, Nat. Mater. 10 (2011) 911–921.
[43] A. Primo, A. Corma, H. Garcia, Phys. Chem. Chem. Phys. 13 (2011) 886–910.
[44] W. Hou, S.B. Cronin, Adv. Funct. Mater. 23 (2013) 1612–1619.
[45] Z.-F. Zheng, J. Teo, X. Chen, H.-W. Liu, Y. Yuan, E.R. Waclawik, Z.-Y. Zhong, H. Zhu, Chem. A: Eur. J. 16 (2010) 1202–1211.
[46] S. Sarina, E.R. Waclawik, H. Zhu, Green Chem. 15 (2013) 1814–1833.
[47] B.K. Min, C.M. Friend, Chem. Rev. 107 (2007) 2709–2724.
[48] D. Widmann, R.J. Behm, Acc. Chem. Res. 47 (2014) 740–749.
[49] D.C. Meier, D.W. Goodman, J. Amer. Chem. Soc. 126 (2004) 1892–1899.
[50] N. Lopez, T.V.W. Janssens, B.S. Clausen, Y. Xu, M. Mavrikakis, T. Bligaard, J.K. Nørskov, J. Catal. 223 (2004) 232–235.
[51] F. Boccuzzi, A. Chiorino, M. Manzoli, P. Lu, T. Akita, S. Ichikawa, M. Haruta, J. Catal. 202 (2001) 256–267.
[52] J.-D. Grunwaldt, M. Maciejewski, O.S. Becker, P. Fabrizioli, A. Baiker, J. Catal. 186 (1999) 458–469.
[53] J.R. Harbour, M.L. Hair, J. Phys. Chem. 82 (1978) 1397–1399.
[54] K. Tanaka, G. Blyholder, J. Phys. Chem. 76 (1972) 3184–3187.
[55] J. Guzman, S. Carrettin, A. Corma, J. Am. Chem. Soc. 127 (2005) 3286–3287.
[56] J. Lunsford, Catal. Rev. 8 (1973) 135–157.